# A LATE QUATERNARY RECORD OF SEASONAL SEA SURFACE TEMPERATURES OFF SOUTHERN AFRICA

Loftus E[a]*, Sealy J[b], Leng MJ[c, d], Lee-Thorp JA[a]

*emma.loftus@rlaha.ox.ac.uk

[a] Research Laboratory for Archaeology and the History of Art, University of Oxford, Dyson Perrins Building, South Parks Road, Oxford, OX1 3QY, UK
[b] Department of Archaeology, University of Cape Town, Private Bag X3, Rondebosch 7701, South Africa
[c] NERC Isotope Geosciences Facilities, British Geological Survey, Keyworth, Nottingham NG12 5GG, UK
[d] Centre for Environmental Geochemistry, School of Geography, University of Nottingham, Nottingham NG7 2RD, UK

ABSTRACT

The southern Cape coastal region is important for understanding both the behavioural history of modern humans, and regional and global climate dynamics, because it boasts a long archaeological record and occupies a key geographical location near the intersection of two major oceans. The western boundary Agulhas Current, implicated in global heat exchange dynamics, is an important modulator of southern African climates and yet we understand its past behaviour only broadly as the Current itself scours the coastal shelf and marine sediment core records necessarily provide little detail. Numerous archaeological sites from both the late Pleistocene and Holocene provide the opportunity for reconstruction of near-shore seasonal SST records, which respond both to localized wind-driven upwellings and Agulhas temperature shifts, corresponding in turn with terrestrial precipitation trends in the near-coastal and summer rainfall regions. Here we present a record of seasonal SSTs extending over MIS5, MIS4, and the Holocene, from serial δ18O measurements of a single gastropod species, Turbo sarmaticus. The results show that mean SST shifts accord well with global SST trends, although they are larger than those recorded in the Agulhas Current from coarser-scale marine sediment records. Comparison with a record of Antarctic sea-ice suggests that annual SST amplitude responds to Antarctic sea-ice extent, reflecting the positioning of the regional wind systems that drive upwelling dynamics along the coast. Thus, near-shore SST seasonality reflects the relative dominance of the westerly and easterly wind systems. These data provide a new climate archive for an important but understudied climate system.

Keywords: Late Pleistocene; Holocene; palaeoclimatology; southern Africa; Agulhas Current; oxygen isotopes; mollusc shells; westerly winds

## Abbreviations

AC – Agulhas Current; BNK1 – Byneskranskop1; HRC – Hoffman's Robberg Cave; KRM – Klasies River Main site; NBC – Nelson Bay Cave; PP5-6 – Pinnacle Point 5-6; SST – sea surface temperature.

## 1 Introduction

The climate of southern Africa is strongly seasonal, with a summer-rainfall climate extending over much of the eastern and northern parts of the subcontinent, and grading into a Mediterranean-like, winter-rainfall climate in the south-west (see Figure 1; Tyson and Preston-Whyte, 2000). The southern Cape lies between these two dominant precipitation regimes and experiences a gradient of rainfall seasonality along its length, and is thus sensitive to shifts in the rain-bearing easterly and westerly wind systems. The coastline, a mixture of rocky and sandy shores subject to high-energy wave action, is adjacent to a large coastal plain, currently submerged but exposed to various degrees in the past depending on global sea levels (van Andel, 1989). Numerous late Pleistocene and Holocene archaeological sites along the coastline of the modern high-sea stand attest to the importance of this coastal shelf region for the history of modern humans.

The Agulhas Current (AC), with an estimated annual transport volume of *c*. 65 Sverdrup, is the largest western boundary current in the Southern Hemisphere (Lutjeharms, 2006), and forms part of the wind-driven circulation of warm tropical waters in the south Indian Ocean. The Current flows from approximately 25°S, along the South African coastal shelf to the southern tip of Africa, where it abruptly retroflects southwards and flows east as the Agulhas Return Current (see Figure 1). At the retroflection, large eddies and rings of warm, salty water occlude off and travel northwards into the South Atlantic Ocean. This leakage of warm Agulhas water into the Atlantic is an important process in the global redistribution of energy via the Atlantic Meridional Overturning Circulation (Beal et al., 2011). The AC is fed mostly by water from a South West Indian Ocean sub-gyre, which circulates in the Agulhas Basin. Some water is also fed in via the Mozambique Current and the East Madagascar Current in the form of intermittent eddies and rings, which contribute to a seasonal signal in the flow of the Agulhas Current (Lutjeharms, 2006).

Cohen and Tyson (1995) presented a theoretical model to interpret near-shore sea surface temperature (SST) records along the southern cape, based on an understanding of the main influences on the regional climate and oceanic systems as reflected in marine mollusc records. According to the model, during periods of increased westerly winds, such as the austral winter when the circumpolar vortex is displaced equator-ward and westerly systems are forced northwards over the southern Cape (Cockcroft et al., 1987), the flow of the Agulhas is weakened and warm waters are advected onshore. At the same time, atmospheric circulation over the southwest Indian Ocean is also weakened and less warm, and moist air is advected over the subcontinent. Consequently, the model predicts that warm surface waters in the Agulhas system and near-shore zone are associated with dry conditions in the interior, summer rainfall zone (”dry-spell mode" – although note that the winter rainfall region will receive more rainfall from the northwards-shifted westerly systems). Conversely, during summer-like conditions when the zone of westerly winds is forced polewards, there is an increased frequency of alongshore easterly-component winds, and surface waters are advected away from the coast by Ekman transport processes. Cooler bottom waters upwell along the in-shore edge of the Agulhas Current, causing the thermocline to rise and leading to rapid drops in coastal SSTs that typically persist for several days (Schumann, 1999; Schumann et al., 1995). These easterly component winds advect warm, moist air over the eastern half of the subcontinent, and bring rainfall to this region. Consequently, the model predicts that cool surface waters along the southern coast during the summer are associated with wet conditions in the summer rainfall zone (“wet-spell mode"). Given the seasonal dimension of this mechanism, with summer SSTs primarily affected by the upwelling processes, shifts in seasonal amplitude can distinguish upwelling-driven SST fluctuations in the near-shore zone from global SST shifts due to glacial/interglacial dynamics.

Cohen and Tyson (1995) also produced a relatively modest dataset of Holocene SST estimates from oxygen isotope analyses of limpet shells preserved at Nelson Bay Cave (see Figure 1) and noted that this dataset seemed consistent with the model described above.

The behaviour of the AC over longer timescales is as yet only poorly understood, despite its important role in global and regional climates. This is in part due to the scarcity of long, finely-resolved archives, as the AC itself scours away much of the sediment from the coastal shelf. Even fewer records reveal details of seasonal conditions in the past, yet seasonality is an important dimension of regional climates, and structures much of the ecological patterning across the subcontinent. The best possibilities for records with the required temporal resolution and chronological control come from material within stratified archaeological sites. Serial oxygen isotope analysis of mollusc shell increments is one of the few proxies of palaeo-SSTs capable of providing robust measures of intra-annual SSTs outside of the tropics (e.g. Carré et al., 2005; Ferguson et al., 2011).

The oxygen isotope composition ($\delta^{18}O$) of calcium carbonate shells reflects both seawater temperature and seawater $\delta^{18}O$ during formation (Urey et al., 1951). Serial sampling of incremental growth layers supplies a record of shifts in marine conditions throughout the growth of the shell. In regions where there are no fluctuations in seawater $\delta^{18}O$, the sequence largely records SST shifts. Mollusc shells are a common component of archaeological sites along the south coast of South Africa, collected by foraging people for food and discarded as refuse that has gradually accumulated in rockshelter and cave deposits. Importantly, such assemblages span tens of thousands of years of occupation in the region, with the same species represented throughout at many sites. The shells are dated by association with the stratified archaeological deposits, which in many cases provides better chronological control than other types of climate archive.

In order to address the gap in our understanding of seasonal variability of Agulhas SSTs over the late Pleistocene and Holocene and the implications for coastal climates, we use archaeological *Turbo sarmaticus* shells from five sites located along the south coast (see Figure 1) to derive seasonally resolved records of near-shore SSTs across the last glacial cycle. Serial $\delta^{18}O$ measurements across the *T. sarmaticus* operculum have been shown to reliably capture mean SST parameters, including the mean annual SST value and the mean annual SST amplitude (Galimberti et al., 2016). Contrasting mean annual SST estimates with the annual SST amplitude (or difference between average SSTs of warmest and coolest months) allows one to distinguish annual SST shifts driven by global climate changes (i.e. glacial/interglacial dynamics) and seasonal effects due to changes in the upwelling regime (described above). The SST record presented here partitions into three broad periods: the first spans much of Marine Isotope Stage (MIS) 5; the second spans the MIS5/4 transition and the final period spans the terminal Pleistocene and the entire Holocene. Thus, this dataset samples both glacial and interglacial conditions and two periods of global climatic transition, providing information about AC seasonal dynamics during large global climate fluctuations.

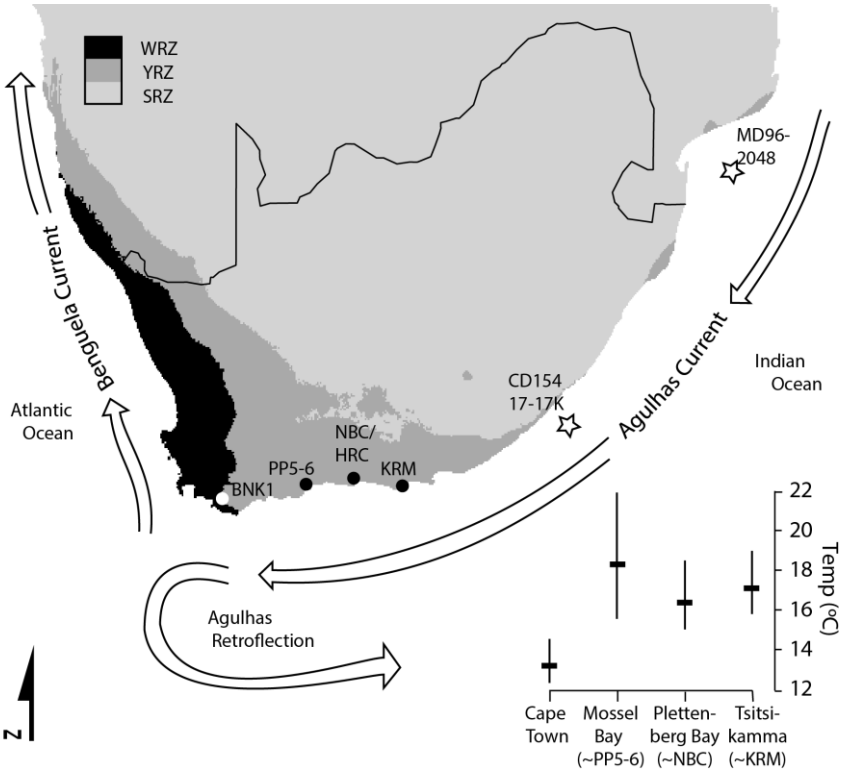


**Figure 1 Map of southernmost Africa, showing the locations of the five archaeological sites in this study (filled circles). Also shown are the modern rainfall zones receiving most (> 66%) annual precipitation in summer (SRZ) and winter (WRZ), and the year-round rainfall zone (YRZ). The major currents are shown schematically, and the position of two off-shore cores is indicated (stars). The plot in the right-hand corner shows the annual mean SSTs at locations along the coast, with the mean annual SST amplitude (mean SST of warmest month – coolest month) indicated by the vertical bar. All SST data 2000-2010 (morning measurements), except at Plettenberg Bay, where 1990-2000 only was available. Data is from the South African Weather Service (www.weathersa.co.za/climate).**

## 2 Material and Methods

### 2.1 Archaeological sites

Samples were obtained from five archaeological sites that span *c*. 500 km of the southernmost coast of South Africa. The distribution of the archaeological sites along the southernmost coast ensures that the temperature records at each are differentially influenced by the oceanographic gradients along this coast (see Figure 1). Samples are from the MIS1 and 2 levels at Nelson Bay Cave (NBC: Deacon, 1986), Hoffman's/Robberg Cave (HRC: Kyriacou 2009) and Byneskranskop 1 (BNK1: Schweitzer and Wilson 1982) and the MIS4 and MIS5 levels of Pinnacle Point 5-6 (PP5-6: Fisher et al., 2015) and Klasies River main site (KRM: Deacon and Geleijnse, 1988; Wurz, 2002). NBC and HRC are located on the same side of the Robberg Peninsula, about 800m apart, and reflect similar environmental conditions. These sites are all caves or rock-shelters located at the modern coastline, except BNK1 which lies *c*. 10 km inland. Deposits are mostly a series of human occupation layers interbedded with aeolian sands, and each site contains well preserved organic material, including shells and faunal remains.

The sites were excavated over the last four decades and the shells used here were largely obtained from museum collections – precise spatial information for each shell is available only at PP5-6, where excavations are ongoing. Thus, samples were aggregated according to broad time periods or

depositional contexts defined by technological or sedimentological features (see Table 1). The archaeological sequences of NBC and BNK1 span the terminal Pleistocene and Holocene (although well-preserved shells are found only in the upper deposits at BNK1), and the chronologies of these two sites are securely underpinned by Bayesian modelled suites of conventional and accelerator radiocarbon dates (Loftus et al., 2016). The recent radiocarbon research at NBC has considerably improved the site's chronology since the study of Cohen and Tyson (1995). Radiocarbon dates from HRC show that the part of the sequence investigated thus far spans only a couple of thousand years in the late Holocene (Kyriacou, 2009). Samples from the three Holocene/ terminal Pleistocene sites are aggregated according to broad time divisions in the Holocene – early (c. 12-8 ka), middle (c. 8 – 4 ka) and later (<4 ka), and the terminal Pleistocene (c. 12 – 14 ka). The KRM deposits are dated by a variety of methods (e.g. optically stimulated luminescence [OSL], electron-spin resonance and U-Th dating), but are constrained only very broadly to periods within MIS5 and samples are aggregated according to the technological units identified by Wurz (2002). The PP5-6 deposits, dated by OSL methods on sediments to periods within MIS5 and MIS4, are well constrained: samples are aggregated according to the depositional units, which are each dated to within a few thousand years (Karkanas et al., 2015).

### *2.2 Turbo sarmaticus* ecology and temperature record

*Turbo sarmaticus* (or giant periwinkle, common name alikreukel) is a member of the globally distributed Turbinidae family known as turban shells, which are characterized by a hard, disc-like, aragonitic operculum that fits into the aperture of the topshell for protection from predators (see Figure 2A). A comparatively large macro-algal grazer endemic to the southern and eastern coasts of South Africa, *T. sarmaticus* is a common component of rocky shore communities along this coastline (Foster, 1997). The species inhabits the lower littoral (intertidal) and sublittoral regions to depths of approximately 8m (Branch et al., 2007). Typically, individuals occupy well-flushed locations and the high energy wave dynamics of this coastline ensure thorough water mixing.

One of the few studies of the life history of *T. sarmaticus* reports a growth rate among wild animals of approximately 25 mm/yr for the topshell and 9 mm/yr for the operculum during the first three years (Foster et al. 1999). The growth rate slows dramatically after this, to *c*. 5 mm/yr and 2 mm/yr for the topshell and operculum respectively. Animals can live up to 10 years (Bruton et al., 1991). The value of *T. sarmaticus* for palaeoenvironmental research derives from the robustness and good preservation of the operculum compared with other shells found in archaeological sites. *T. sarmaticus* opercula are frequently preserved largely intact, unlike thin-shelled topshells, bivalves and limpets, and form a significant component of south coast archaeological assemblages spanning the last glacial cycle (e.g. Langejans et al. 2012).

The *T. sarmaticus* operculum does however present challenges for seasonal-resolution sampling as many commonly used sclerochronological methods cannot be applied. The portion of the operculum with regular growth increments is just a few millimetres thick, so the operculum cannot be sectioned or polished prior to sampling and must be sampled directly from the ridged surface. Annual growth patterns are not clearly identifiable, and the growth of the opercula is slow relative to many species used in similar studies, limiting the number of samples per annual cycle and the possibility of using statistical curve-fitting approaches to reconstruct seasonality. Additionally, the direction of growth changes abruptly throughout life as the animal rotates the operculum to better fit the aperture of the coiling topshell during growth (see Figure 2).

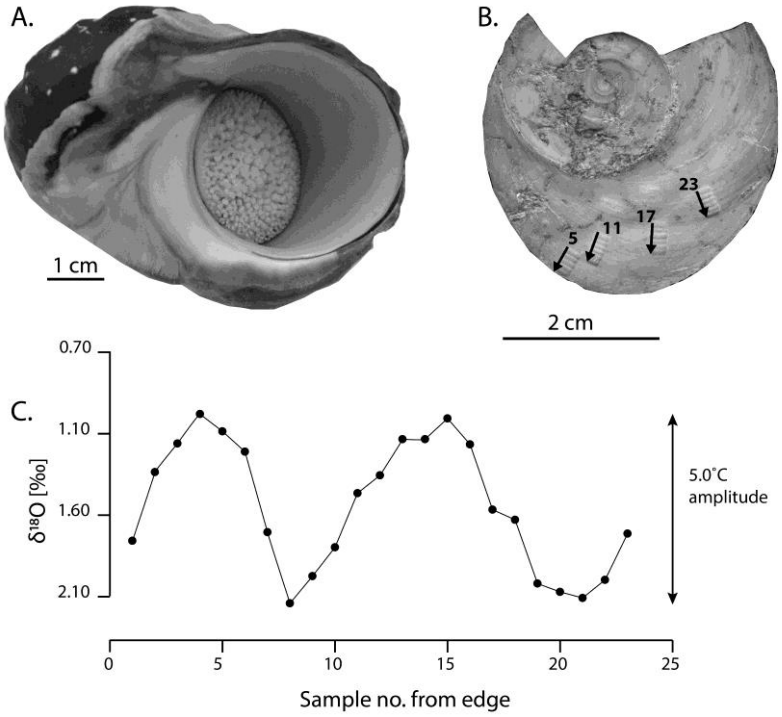


**Figure 2 (A) *Turbo sarmaticus* shell with operculum pulled into aperture; (B) Inner surface of broken archaeological *T. sarmaticus* operculum from PP5-6 (ID PP131492 from context SADBS, 71 ± 3 ka) with 23 micromilled samples (numbered), arrows indicating the changing direction of growth and sampling path; and (C) $\delta^{18}O$ measurements of PP131492, showing the seasonal SST signal, with the annual SST amplitude indicated.**

Notwithstanding the complexity of the growth patterns, earlier studies have indicated the utility of this species for archaeological research and palaeotemperature reconstruction. Shackleton (1982) analysed $\delta^{18}O$ of a small number of opercula from KRM; his purpose was to establish a chronology for the shell midden based on the global sea-level curve. Henshilwood (2008) measured archaeological *T. sarmaticus* $\delta^{18}O$ to explore changes in the seasonal timing of shellfish harvesting during the Holocene. Most recently, Galimberti et al. (2016) undertook a systematic study of modern *T. sarmaticus* opercula, collected from Mossel Bay between 2004-2007, to determine the reliability of temperature records from this species. The data show that *T. sarmaticus* precipitate their shells in equilibrium with water temperature and the Grossman and Ku (1986) palaeotemperature equation for all carbonates (as modified by Hudson and Anderson (1989) to account for the 0.2‰ difference between SMOW and average marine water) is most appropriate for this species:

$$T\ (°C) = 19.7 - 4.34*(\delta^{18}O_{aragonite} - \delta^{18}O_{water}),$$

where the $\delta^{18}O_{water}$ value is 0.52‰, as established by modern measurements at Mossel Bay (Galimberti et al., 2016).

The modern data of Galimberti et al. (2016) show that although single individuals do not necessarily capture the full annual temperature amplitude recorded by *in situ* thermometers, *mean* SST parameters that represent typical conditions are accurately represented across a set of opercula. Thus, the average shell-derived maximum (22.3°C) and minimum (15.6°C) SSTs match well with the actual mean temperatures of the warmest and coolest months at Mossel Bay between 2000-2007 (Jan = 22.4°C; Jul = 15.6°C). Consequently, the amplitude of SSTs from each shell averaged across the

full set of shells, 6.7°C, corresponds well with the average seasonal range of measured SSTs at Mossel Bay (6.8°C; i.e. the difference between the mean temperatures of the warmest and the coolest months).

Although it has been suggested that a truncated SST amplitude recorded in individual modern *T. sarmaticus* opercula might reflect physiological temperature limits for *T. sarmaticus* (i.e. temperatures above and below which they cannot grow), examination of archaeological data from an MIS5 site (Pinnacle Point 13b) suggests that this is not the case as these shells record cooler temperatures than the modern lower limit (data reported in a doctoral thesis; Galimberti, 2010). Additionally, the modern habitat of *T. sarmaticus* extends to the markedly cooler Atlantic waters around the Cape Point peninsula (annual average SST = 13.3°C; Branch et al., 2007). These observations suggest that the attenuated SST amplitude recorded in individual opercula might reflect either a physiological limit on time spent growing driven by their biological clocks, and that the animals can in fact shift their temperature tolerances to some degree, or rather that the sampling resolution of the Galimberti et al. (2016) study was simply inadequate to capture periods of slower growth during stressful growth seasons.

The approach taken here, where data from several archaeological opercula per context is aggregated to determine mean SST statistics, offers improved potential to capture the general environmental conditions compared with studies based on single shells per time unit, where microhabitat signals or stressful events in the life-histories of individual molluscs may introduce bias. Where climate is considered as the average state of environmental conditions aggregated over several decades, palaeoclimate records from high-resolution but short-lived archives such as mollusc shells require appropriately conservative interpretation.

### 2.3 Shell selection and sampling

*T. sarmaticus* precipitate their opercula as aragonite, a polymorph of $CaCO_3$ that is metastable under atmospheric conditions and is more vulnerable to dissolution and recrystallization than calcite, thus erasing the original oxygen isotope record in the process. Aragonitic shells provide an inherent advantage over calcitic shells for palaeoclimate reconstructions in that, while the potential for dissolution and recrystallisation is greater, the detection of calcite provides an unambiguous indication of recrystallization and altered shells can be removed from analysis. A greater challenge for this study is the patchy occurrence of diagenesis over the exposed surface of the opercula from which the growth increments are sampled. This variability of preservation within a single operculum demands a highly resolved assessment of recrystallization across the entire drilling path. In order to overcome this problem we applied a method based on Fourier transform infrared spectroscopy with an attenuated reflectance attachment (FTIR-ATR) to small aliquots (c. 0.5 mg) of powdered sample to test for and quantify the presence of calcite in several samples from each operculum (Loftus et al., 2015). Opercula were pre-screened using this method, whereupon approximately a quarter of the opercula were discarded, although this varied between the older, Pleistocene sites and the Holocene-aged sites where preservation was generally better. Upon micromill sampling, approximately every $4^{th}$ or $5^{th}$ milled sample (i.e. 2 - 3 mm) was screened with FTIR-ATR, and if recrystallisation was detected along the drilling path then the series of powdered samples continuing past the altered patch were discarded. Approximately a fifth of the milled samples from all sites were discarded in this way.

**Table 1 All sample contexts, correction for global changes in oceanic $\delta^{18}O$ averaged across the age range for each context (based on Waelbroeck et al., 2002), and the numbers of samples analysed. Holocene sub-contexts from NBC, BNK1 or HRC are distinguished by the first letter N, B or H, respectively. Calibrated radiocarbon dates for NBC and BNK1 in Loftus et al. (2016), and for HRC in Kyriacou (2009). OSL ages for PP5-6 in Karkanas et al. (2015), KRM dated with various methods, see Wurz (2002). Welch's unequal variances t-test results for significant differences between opercula from the same sub-context are indicated (*: p<0.05; **: p<0.001; data were tested for normality).**

| | Context | Sub-contexts | Date (ka) | $\delta^{18}O$ correction (‰) | No. of opercula | No. of $\delta^{18}O$ samples |
|---|---|---|---|---|---|---|
| NBC, HRC and BNK1 | Late Holocene < 4.2 ka | Sub-total | | | 7 | 104 |
| | | B_1_Eva | 1.7-1.9 | 0 | 1 | |
| | | N_EIII | 2.5 | 0 | 2 | |
| | | B_4_Dud | 3.7-4.0 | 0 | 2 | |
| | | H_RR_P | 4.0-4.3 | 0 | 2 | |
| | Mid Holocene *c*. 4.2 - 8.2 ka | Sub-total | | | 9 | 159 |
| | | B_5_Inge | 3.9-6.1 | 0.03 | 1 | |
| | | N_Ivan** | 4.9-6.6 | 0.03 | 2 | |
| | | B_6_Hilary | 6.1-6.6 | 0.04 | 1 | |
| | | N_Glen | 5.9-7.0 | 0.06 | 1 | |
| | | B_9_Mort** | 6.4-7.4 | 0.06 | 2 | |
| | | N_RiceA | 6.8-9.2 | 0.15 | 2 | |
| | Early Holocene *c*. 8.2 - 11.9 ka | Sub-total | | | 8 | 165 |
| | | N_RiceB* | 9.2-9.7 | 0.21 | 2 | |
| | | N_Jake | 9.5-11.4 | 0.30 | 4 | |
| | | N_BSBJ** | 10.9-11.9 | 0.48 | 2 | |
| | End Pleistocene | N_GSL** | 12.0 - 14.9 | 0.75 | 3 | 65 |
| PP5-6 | DBCS | | 62 ± 3 | 0.54 | 1 | 20 |
| | OBS1 | | 69 ± 3 | 0.64 | 5 | 80 |
| | SADBS | | 71 ± 3 | 0.58 | 8 | 151 |
| | ALBS | | 72 ± 3 | 0.51 | 5 | 74 |
| | LBSR | | 81 ± 4 | 0.22 | 5 | 74 |
| KRM | MSA II Upper | | c. 80 - 85 | 0.22 | 7 | 104 |
| | MSA II Lower | | c. 90 - 95 | 0.32 | 8 | 112 |
| | MSA I | | c. 115-120 | 0.07 | 6 | 67 |
| | Total | | | | 72 | 1175 |

After pre-screening, opercula were micromilled using a New Wave Merchantek micromill with tungsten carbide dental burrs (0.8 mm – overlapping of samples allows for *c*. 0.6 mm resolution). Samples were taken in a nested series of curved lines that lie perpendicular to the direction of growth. This sampling strategy is unlike previous sampling efforts: continuous, curving arcs of individual holes that followed the mid-line of the operculum (Galimberti et al., 2016; Henshilwood, 2008; Shackleton, 1982). Rather, the direction of sampling is shifted in accordance with the direction of growth changes, forming sets of discontinuous, but overlapping, samples (see Figure 2B). The number of analytical samples per operculum ranges from 5 to 26, depending on size and preservation of the shell.

Twenty-seven opercula were sampled from the three Holocene sites (including the terminal Pleistocene deposits at NBC), and 45 from the Late Pleistocene sites, 24 from PP5-6 and 21 from KRM (see Table 1). Table 1 also shows the age for each context and sub-context where this can be resolved, and the correction applied for changes in global ocean $\delta^{18}O$ across the glacial cycle according to Waelbroeck et al. (2002). The error of the correction is a result of the age uncertainty of the sample in each case.

### 2.4 Analyses

Carbonate samples with < 10% calcite were analysed on one of three systems (indicated in Table SM1) - a Kiel Device coupled to a Delta V Advantage isotope mass spectrometer in the Earth Science Department, University of Oxford (external reproducibility of 0.10‰ for $\delta^{18}O$); an automated Thermo GasBench II device, coupled to a Thermo Delta V Advantage isotope mass spectrometer at the Division of Archaeological, Geographical and Environmental Sciences of the University of Bradford (external reproducibility of 0.30‰ for $\delta^{18}O$); and a Multiprep device coupled to a GV Isoprime isotope mass spectrometer at the NERC Isotope Geosciences Facilities at the British Geological Survey, Keyworth (external reproducibility of <0.10‰ for $\delta^{18}O$). In each case $CO_2$ was produced by 100% phosphoric acid hydrolysis, and the solid-gas fractionation of the samples is corrected using an aragonite specific factor with appropriate corrections for reaction temperature (1.00906 at 71°C [Kiel and Gasbench], 1.00854 at 90°C [Isoprime]; Kim et al., 2007). For the calculation of temperatures from a carbonate palaeotemperature equation (Grossman and Ku, 1986), however, the $\delta^{18}O$ values are adjusted for solid-gas fractionation using a calcite-specific factor (1.00868 at 71°C, 1.00813 at 90°C; Kim et al., 2007) as the Grossman and Ku (1986) study did not take into account the differing fractionation factors (see also Füllenbach et al., 2015) – accordingly, both sets of $\delta^{18}O$ values are reported to aid comparison between studies. The samples were calibrated against internal calcite standards calibrated in turn to international standards (NBS19: $\delta^{18}O$=–2.20‰). Results are reported in the delta-notation relative to V-PDB, according to the equation:

$$\delta^{18}O\ (‰) = \{(R_{SAMPLE})/ (R_{STANDARD})–1\} \times 1000,$$

where $R_{SAMPLE}$ and $R_{STANDARD}$ is the $^{18}O/^{16}O$ ratio of the sample and reference materials.

**Figure 3 Scatterplot showing linear regression model of mean $\delta^{18}O$ value for each shell against the amplitude of $\delta^{18}O$ values per shell.**

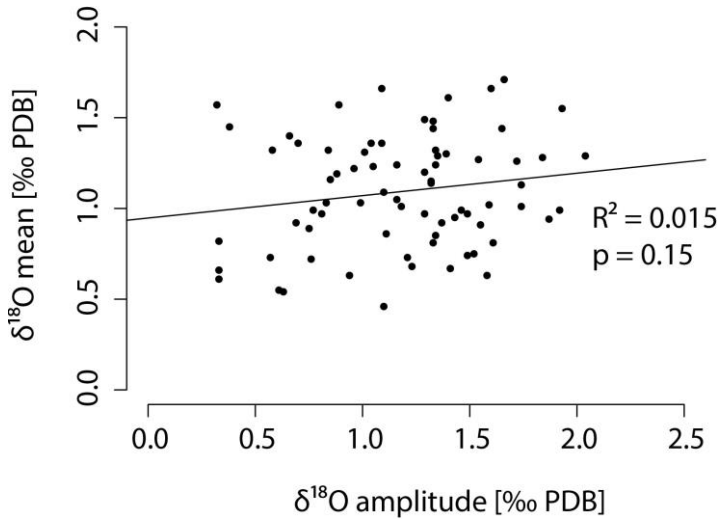

**Table 2** Summary statistics for *Turbo sarmaticus* $\delta^{18}O$ data from all archaeological contexts (see supplementary table for data), with reconstructed temperatures using the Grossman and Ku (1986) equation for all data (as modified by Hudson and Anderson (1989)). $\delta^{18}O$ values are shown adjusted for solid-gas fractionation using an aragonite specific factor, and a calcite factor for application in the palaeotemperature (PT) equation, (resulting in values *c.* 0.4‰ more positive). The $\delta^{18}O_{water}$ value for the equation is 0.52‰, adjusted by the change in global ocean $\delta^{18}O$ for each context, as recorded in Table 1. Also shown are the data from modern opercula collected by Galimberti et al. (2016) and the departures between the modern and archaeological data. The averaged parameters from each level are calculated from the maximum, minimum and amplitude of each operculum from that level (see section 2.2), and so cannot be calculated for DBCS at PP5-6, where only one operculum was available.

| | | | Number of analyses | Number of shells | Mean | Ave. max $\delta^{18}O$ / Ave. min T(°C) | Ave. min $\delta^{18}O$ / Ave. max T(°C) | Ave. ampli-tude |
|---|---|---|---|---|---|---|---|---|
| | Modern | $\delta^{18}O$ (‰) | 327 | 16 | +0.69 | +1.47 | -0.07 | |
| | | T(°C) conversion | | | 19 | 15.6 | 22.3 | 6.7 |
| NBC, BNK1 and HRC | Late Holocene | $\delta^{18}O$ (‰) | 104 | 7 | +1.06 | +1.56 | +0.46 | |
| | | PT $\delta^{18}O$ (‰ ) | | | +1.44 | +1.96 | +0.85 | |
| | | T(°C) conversion | | | 15.7 | 13.5 | 18.3 | 4.8 |
| | | T(°C) dep. from modern | | | -3.3 | -2.1 | -4.0 | -1.9 |
| | Mid Holocene | $\delta^{18}O$ (‰) | 159 | 9 | +1.27 | +1.70 | +0.73 | |
| | | PT $\delta^{18}O$ (‰ ) | | | +1.67 | +2.09 | +1.11 | |
| | | T(°C) conversion | | | 14.7 | 12.9 | 17.1 | 4.2 |
| | | T(°C) dep. from modern | | | -4.3 | -2.7 | -5.1 | -2.5 |
| | Early Holocene | $\delta^{18}O$ (‰) | 165 | 8 | +1.58 | +2.16 | +0.91 | |
| | | PT $\delta^{18}O$ (‰ ) | | | +1.96 | +2.55 | +1.29 | |
| | | T(°C) conversion | | | 13.4 | 10.9 | 16.3 | 5.4 |
| | | T(°C) dep. from modern | | | -5.5 | -4.7 | -5.9 | -1.2 |
| | Late Pleistocene | $\delta^{18}O$ (‰) | 65 | 3 | +2.03 | +2.78 | +1.21 | |
| | | PT $\delta^{18}O$ (‰ ) | | | +2.38 | +3.17 | +1.60 | |
| | | T(°C) conversion | | | 11.6 | 8.2 | 15.0 | 6.8 |
| | | T(°C) dep. from modern | | | -7.3 | -7.4 | -7.3 | 0.1 |
| PP5-6 | DBCS | $\delta^{18}O$ (‰) | 20 | 1 | +1.48 | | | |
| | | PT $\delta^{18}O$ (‰ ) | | | +1.89 | - | - | |
| | | T(°C) conversion | | | 13.8 | - | - | - |
| | | T(°C) dep. from modern | | | -5.2 | - | - | - |
| | OBS1 | $\delta^{18}O$ (‰) | 80 | 5 | +1.66 | +2.38 | +0.91 | |
| | | PT $\delta^{18}O$ (‰ ) | | | +2.07 | +2.79 | +1.32 | |
| | | T(°C) conversion | | | 13.0 | 9.9 | 16.2 | 6.4 |
| | | T(°C) dep. from modern | | | -6.0 | -5.7 | -6.0 | -0.3 |
| | SADBS | $\delta^{18}O$ (‰) | 151 | 8 | +1.34 | +1.99 | +0.75 | |
| | | PT $\delta^{18}O$ (‰ ) | | | +1.75 | +2.40 | +1.16 | |
| | | T(°C) conversion | | | 14.3 | 11.5 | 16.9 | 5.4 |
| | | T(°C) dep. from modern | | | -4.6 | -4 | -5.3 | -1.3 |
| | ALBS | $\delta^{18}O$ (‰) | 74 | 5 | +1.49 | +1.81 | +1.04 | |
| | | PT $\delta^{18}O$ (‰ ) | | | +1.90 | +2.22 | +1.45 | |
| | | T(°C) conversion | | | 13.7 | 12.3 | 15.7 | 3.4 |
| | | T(°C) dep. from modern | | | -5.2 | -3.3 | -6.6 | -3.3 |
| | LBSR | $\delta^{18}O$ (‰) | 74 | 5 | +1.02 | +1.53 | +0.48 | |
| | | PT $\delta^{18}O$ (‰ ) | | | +1.43 | +1.94 | +0.89 | |
| | | T(°C) conversion | | | 15.7 | 13.5 | 18.1 | 4.6 |
| | | T(°C) dep. from modern | | | -3.2 | -2.1 | -4.2 | -2.1 |
| KRM | MSAII | $\delta^{18}O$ (‰) | 104 | 7 | +1.57 | +2.27 | +0.91 | |

| | | | | | | | |
|---|---|---|---|---|---|---|---|
| upper | PT $\delta^{18}O$ (‰ ) | | | +1.98 | +2.68 | +1.32 | |
| | T(°C) conversion | | | 13.3 | 10.3 | 16.2 | 5.9 |
| | T(°C) dep. from modern | | | -5.6 | -5.3 | -6.0 | -0.8 |
| MSAII lower | $\delta^{18}O$ (‰) | 112 | 8 | +1.60 | +2.09 | +0.96 | |
| | PT $\delta^{18}O$ (‰ ) | | | +2.01 | +2.50 | +1.37 | |
| | T(°C) conversion | | | 13.2 | 11.1 | 16.0 | 4.9 |
| | T(°C) dep. from modern | | | -5.7 | -4.5 | -6.2 | -1.7 |
| MSAI | $\delta^{18}O$ (‰) | 67 | 6 | +1.43 | +1.88 | +0.76 | |
| | PT $\delta^{18}O$ (‰ ) | | | +1.84 | +2.29 | +1.17 | |
| | T(°C) conversion | | | 14.0 | 12.0 | 16.9 | 4.9 |
| | T(°C) dep. from modern | | | -5.0 | -3.6 | -5.4 | -1.8 |

## 3 Results

A total of 1175 $\delta^{18}O$ samples from 72 archaeological opercula were analysed (Table 1). The raw isotope measurements, uncorrected for changes in global ocean $\delta^{18}O$, but corrected for solid-gas fractionation using both aragonitic and calcitic (for palaeotemperature conversions) appropriate correction factors are provided in supplementary material (Table SM1 and SM2). The serial isotope profiles of many opercula produce seasonal cycles as expected (see Figures 2, SM1, SM2 and SM3). The key $\delta^{18}O$ and converted temperature statistics for each context are provided in Table 2. Figure 3 shows average $\delta^{18}O$ values for each shell compared with the total $\delta^{18}O$ amplitude for that shell using raw $\delta^{18}O$ values. The lack of a strong relationship (adjusted $R^2$ = 0.015; p-value = 0.1494) between mean SST and SST amplitude per shell supports the hypothesis that there is no bias against growth under cool climate conditions and allows interpretation of changes in seasonal amplitude across the glacial cycle.

**Figure 4 Boxplots of *Turbo sarmaticus* $\delta^{18}O$ values from each archaeological context (Table 2) with sites indicated. Numbers of shells are shown below each box, with the number of analytical samples in brackets. Note the left-hand scale has been reversed so that the top of the graph reflects higher temperatures. Significant results for pairwise statistical comparisons are indicated by ** (p<0.001; Post-hoc TukeyHSD test).**

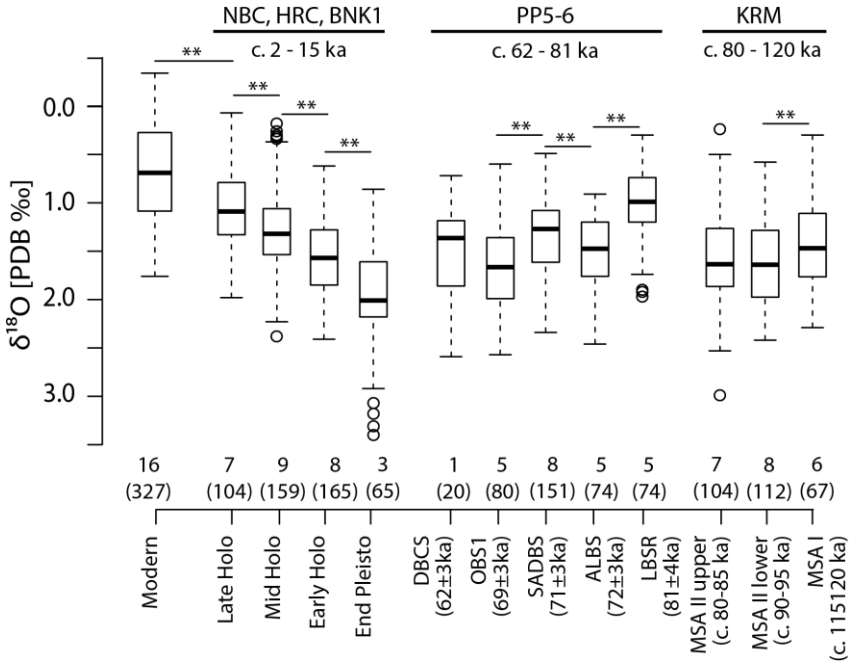

### 3.1 Glacial-interglacial shifts in near-shore seasonal SST record

The aggregated $\delta^{18}O$ measurements for each stratigraphic excavation unit are shown in Figure 3. The data show clear shifts in mean SST and annual SST amplitude. Across the terminal Pleistocene and Holocene, the shell-derived SSTs reflect a steady warming of 4.1°C (see also Figure 5), while a more variable pattern of SST change is recorded across the MIS5/4 transition, with SSTs declining by 2.7°C overall from the oldest level at PP5-6, LBSR (82 ± 4 ka), to level OBS1 (82 ± 3 ka). At KRM, the SST record is considerably more stable, reflecting less than 1°C change across the three time periods.

The record also shows shifts in seasonality as recorded in the annual SST amplitude. During all three periods of the Holocene, mean minimum temperatures differ less from the modern dataset of Galimberti et al. (2016) than do the mean maximum temperatures. For example, during the late Holocene, the averaged minimum recorded SSTs are 2.1°C cooler than recorded by the modern dataset, but the averaged maximum recorded SSTs are 4.0°C cooler. This asymmetry in the departures between maximum and minimum temperatures suggests that during this period cooler summer SSTs had more of an effect on the overall temperature shifts than did the cooler winter SSTs. Arguably, this pattern of cooler maximum SSTs could simply reflect biased growth trends of *T. sarmaticus*, as the species might sufficiently slow its growth under cool conditions so that winter SST values are underrepresented. However, this interpretation is directly challenged by the data from the terminal Pleistocene levels, where the departure from modern was approximately equal (c. 7.3°C) in the averaged maximum and minimum SSTs, indicating that at this time the cooling was more or less equally distributed throughout the year.

Figure 7(F) shows the annual average SST amplitude across all the data, which, for the terminal Pleistocene/Holocene dataset, is lowest during the mid-Holocene (4.2°C) and highest during the terminal Pleistocene (6.8°C). The situation is mirrored for the MIS5/4 data from PP5-6, where the annual SST amplitude is high in the glacial MIS4 assemblage in context OBS1 (69 ± 3 ka: 6.4°C) and lower during the interglacial MIS5 assemblages in contexts LBSR (81 ± 4 ka: 4.6°C) and ALBS (72 ± 3 ka: 3.4°C) especially (date ranges in Karkanas et al., 2015). Similar to the Holocene dataset, the low annual amplitudes in the PP5-6 dataset are driven by cooler maximum temperatures during both LBSR and ALBS, which are depressed by approximately twice as much as the minimum temperatures compared with modern values. During early MIS4 glacial OBS1, SSTs are depressed by *c*. 5.7 – 6.0°C year round, which is similar to the SST depression observed during the terminal Pleistocene.

### 3.2 Intra-context variability

Chronological control among the Holocene-aged samples is sufficient to permit $\delta^{18}O$ correction according to the age of the sub-context (see Table 1), allowing exploration of variability in SST estimates at finer timescales. More than one shell was measured from a single stratigraphic excavation unit or sub-context in ten instances (see Table 1), and significant differences are observed in five cases (with Welch two sample t-test for unequal sample sizes: significant results indicated in Table 1). These differences may reflect climatic changes occurring within the timespan represented by the stratigraphic sub-context or micro-scale differences in the habitats of individual *T. sarmaticus*. It is worth noting that only in one of these ten sub-contexts, where age estimates can span thousands of years, does the standard deviation among $\delta^{18}O$ analyses exceed that recorded among all sixteen modern shells collected over just a few years (0.52‰, versus that of 0.56‰ during the terminal Pleistocene), and where the standard deviation presumably results from small differences in annual SSTs and microhabitat. Where two or more shells from a single depositional

unit reflect similar mean temperatures, one can infer with greater confidence that the shells record average environmental parameters rather than microhabitat conditions. Yet, as demonstrated by the modern study of Galimberti et al. (2016), analysis of multiple shells allows for more accurate reconstruction of parameters such as mean SST and seasonal amplitude.

Figure 5 shows the shell-derived SSTs for the Holocene and terminal Pleistocene dataset, according to sub-context. The same overall trends are evident as in Figure 4, although the magnitude of SST shifts within each context are now clear. For example, during the mid-Holocene, SSTs at NBC fluctuate by over 2°C from sub-context Rice A (14.0°C; 6.8-9.2 kcalBP, n=29) to Ivan (16.4°C; 4.9-6.6 kcalBP, n=33), whereas SSTs change less than 1°C across the early Holocene from sub-context BSBJ (13.1°C; 10.9-11.9 kcalBP, n=46) to Rice B (13.7°C; 9.2-9.7 kcalBP, n=40), suggesting that the mid-Holocene witnessed more dynamic conditions in the near-shore zone that did the early Holocene. Similar assessments of intra-context variability will be possible further back in time at KRM and PP5-6, as ongoing dating efforts at these sites improve the age estimates for the depositional contexts and allow for more precise and accurate corrections for changes in ocean $\delta^{18}O$.

**Figure 5 Boxplots of *Turbo sarmaticus* shell $\delta^{18}O$ derived temperatures by sub-unit and site for Holocene and terminal Pleistocene aged samples (see Table 1 for contextual information). Dotted horizontal lines indicate average temperature for the entire period. Number of analytical samples and number of shells (in brackets) per unit is shown above each unit. Temperatures calculated using the Grossman and Ku (1986) equation for all carbonates, as modified by Hudson and Anderson (1989).**

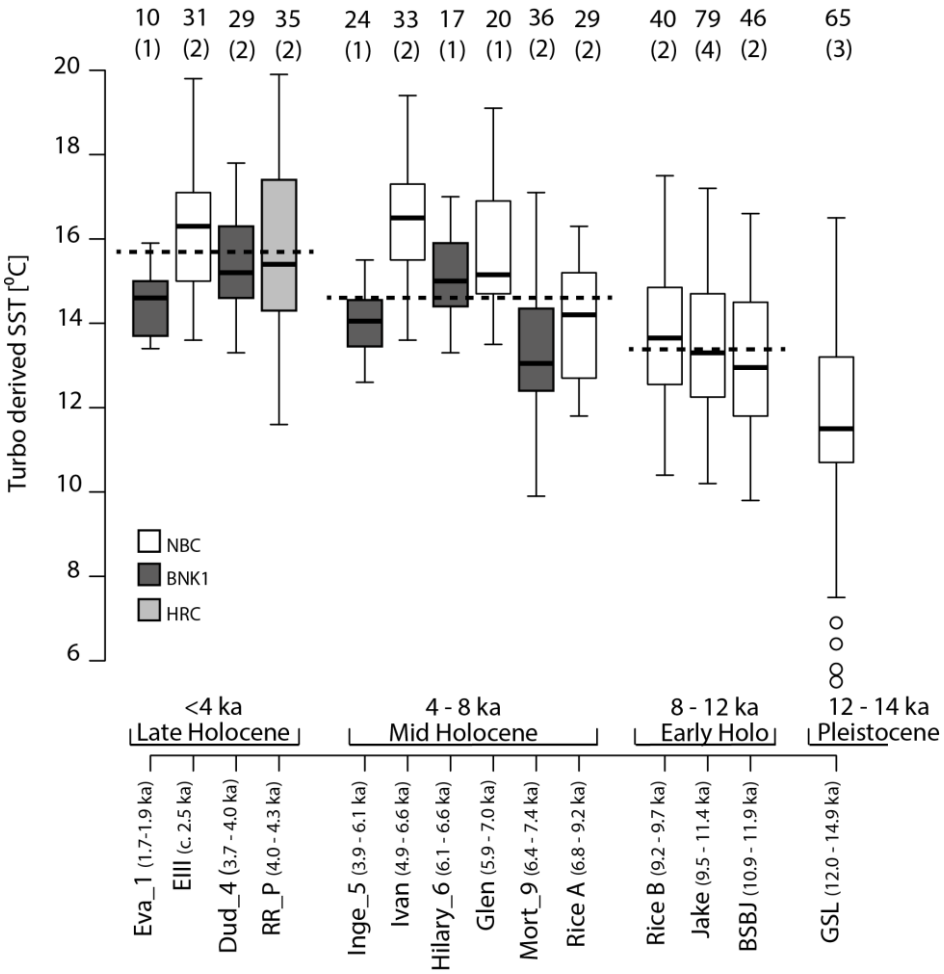

### 3.3 Spatial variation in near-shore SSTs

Along-shore SST trends can be reconstructed for the mid-late Holocene and at *c*. 82 ka, as data from two geographically separated sites overlaps during these intervals. In the mid and late Holocene, shell-derived SSTs from the Robberg Peninsula (NBC and HRC) are consistently higher than those from BNK1, consistent with modern SST gradients between Plettenberg Bay (see Figure 6: instrumental mean SST = 16.4°C; annual range = 3.6°C) and Cape Town, to the west of BNK1 (instrumental mean SST = 13.3°C; annual range = 2.3°C: data available on request from South African Weather Service). During the mid-Holocene, reconstructed mean annual SSTs at BNK1 are 13.9°C and on the Robberg Peninsula 15.4°C; the average amplitude at both locations is the same (4.2°C). During the late Holocene, the mean annual SST at BNK1 is 15.1°C, while that at Robberg is 16.0°C. The average amplitude differs sharply between BNK1 (3.4°C) and the Robberg Peninsula (5.9°C).

At *c*. 82 ka, SSTs at KRM are 13.3°C, while those at PP5-6 are 15.7°C. This, too, is consistent with the modern SST gradient, as instrumental temperatures recorded at Tsitsikamma, near to KRM, today average 17.1°C, while those at Mossel Bay average 18.4°C. However, the average amplitude is only 4.6°C in level LBSR at PP5-6, while it is 5.9°C in the MSA II upper level at KRM. To contrast, the modern annual SST range at Mossel Bay is 6.7°C and that at the Tsitsikamma SST station is 3.1°C. The large SST range at Mossel Bay today is driven largely by very warm summer SSTs: conversely, the high SST amplitude at KRM at 82 ka appears to be largely a result of very low winter SSTs, averaging 10.3°C at this time.

**Figure 6 Mean shell-derived SST values by location along the south coast and by time period, with modern SSTs (*in-situ* measurements available on request from South African Weather Service). The mean annual temperature amplitude (i.e. difference between averaged maximum and minimum temperatures) for each dataset is indicated by the vertical lines.**

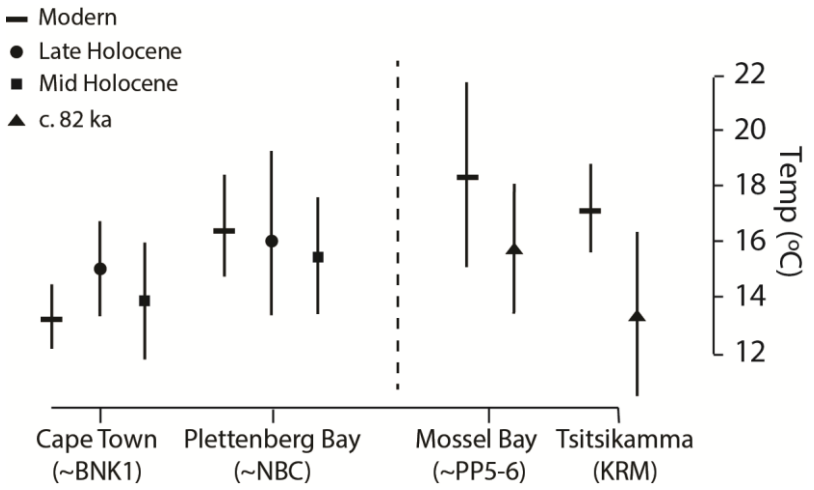


## 4 Discussion

### 4.1 Agulhas Current and near-shore SST trends

The spatial patterns between the sites and the temporal shifts in temperature match well with both the modern spatial temperature gradient along this coastline, and global climate shifts across MIS5 through the late Holocene, although our data represent but a small number of annual seasonal cycles across each depositional unit. The clearest SST trend is the steady rise in temperatures from the terminal Pleistocene through the Holocene. The PP5-6 data shows a gradual decline in temperatures between 82 ± 4 ka (LBSR) and 69 ± 3 ka (OBS1), although the trend is not linear,

suggesting that fluctuations in local SST and oceanographic conditions accompanied the transition from interglacial to glacial conditions between MIS5 and MIS4. In contrast, the MIS5 dataset from KRM shows relatively little change between the three levels. This stability might indicate that the site was occupied only during MIS5 interstadials, which is consistent with the broad dates for the deposits.

Figure 7 shows a measure of regional climate seasonality (the difference between June and December insolation; Berger and Loutre, 1991), alongside a stacked record of AC SSTs for the last 115 ka from marine sediment core MD96-2048, located in the formation region of the AC adjacent to the Delagoa Bight (Caley et al., 2011); and a record of AC SSTs for the last 100 ka derived from marine sediment core CD154 17-17K located in the main trajectory of the AC (Simon et al., 2013). The SST estimates by Simon et al. (2013) are derived via a similarity index transfer function based on modern analogue foraminiferal assemblages, which allows for the estimation of summer and winter SSTs in addition to an annual average. Both the MD96-2048 and CD154 17-17K temperature estimates are for off-shore locations closer to the Indian Ocean, and so are not directly comparable with the shell-derived records of this study, which, in addition to responding to the SST shifts of the larger AC system, are also influenced by near-shore processes such as upwelling. These core records, however, provide information about the long-term behaviour of the Agulhas system (Caley et al., 2011), and their juxtaposition with the shell-derived SST records allows us to discern global and regional processes. Also shown in Figure 7 is an Antarctic record of sea salt sodium concentrations, a measure of polar sea-ice extent, which effects the position of the hemispheric wind belts (Fischer et al., 2007). These measures of seasonality, Agulhas Current conditions and hemisphere-wide atmospheric dynamics are displayed alongside the shell-derived mean SST reconstructions (mean, maximum and minimum per context) and shell-derived SST amplitudes (see Table 2).

**Figure 7 Shell-derived SSTS by depositional unit against: A) insolation seasonality (June-December insolation) at 30°S (Berger and Loutre, 1991); B) AC SSTs derived from Mg/Ca ratios and alkenone and tetraether indices from marine core MD96-2048 (26° 10.0'S, 34° 1.0'E; Caley et al., 2011); C) planktic foraminifera derived AC seasonal SSTs from marine sediment core CD154 17-17K (33° 19.2'S, 29° 28.2'E; Simon et al., 2013) with five point running averages overlaid, and D) sea salt sodium concentrations from EPICA DML ice-core as a measure of sea ice extent (Fischer et al., 2007). E) Shell-derived SSTs are shown with average maximum and minimum values and the F) range between these values is plotted below. Robberg sites (NBC and HRC only: BNK1 values not included here): diamonds; PP5-6: circles; and KRM: squares. Note that the data from PP5-6 unit DBCS are not shown as they derive from only a single shell.**

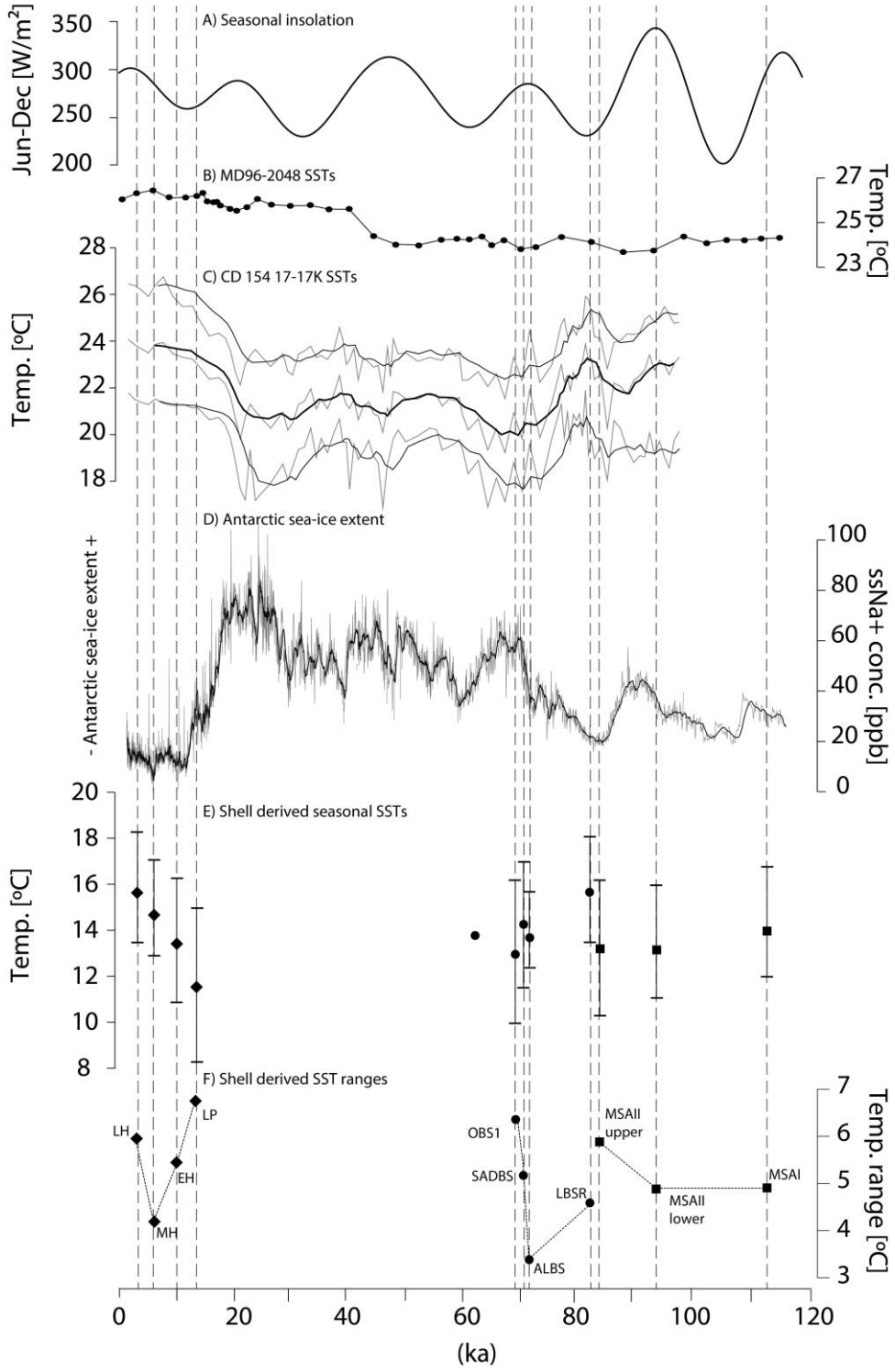

Neither the shell-derived average SSTs nor the annual SST amplitudes correspond with seasonal insolation, suggesting that other mechanisms drive the large shifts in SST and seasonality in the Agulhas and near-shore zone. While reconstructions of AC SSTs from offshore cores are considerably warmer than those reflected in the shell records, the magnitude of SST shifts is muted in the main Agulhas system compared with the near-shore zone (SSTs are displayed at the same scale in Figure 5). Moreover, the fluctuations in seasonal temperature amplitudes reported by Simon et al. (2013) are more constrained (between 4.0 - 5.6°C) compared to those from shell records (3.4 - 6.8°C), suggesting that seasonal amplitude in the main AC may be buffered from the processes that influence SST shifts and seasonal amplitude in the near-shore SST record. Admittedly, the marine core records are likely to be time averaged from mixing and bioturbation processes, dampening any large changes in annual SST.

The seasonal amplitude of nearshore SSTs corresponds well with a record of sea-ice extent from Antarctica (Fischer et al., 2007). During the terminal Pleistocene, when sea-ice was more extensive than during the Holocene, the larger seasonal amplitude of near-shore SSTs indicates summer upwelling was reduced. As sea-ice extent is known to affect the position of the dominant wind systems around southern Africa (Chase et al., 2015), this relationship suggests that the south coast experienced reduced frequency of the easterly winds that drive summer upwelling of cooler, deeper water, as the austral westerly wind systems were forced equatorwards over the southern part of South Africa. Conversely, during the mid-Holocene, the low amplitude of the near-shore SST reconstructions argues for enhanced summer upwelling, when sea-ice extent in the Atlantic sector of the Southern Ocean is most diminished (Fischer et al., 2007). Sea-ice extent around Antarctica subsequently expanded about 5 ka through the late Holocene (Fischer et al., 2007), when the higher late Holocene shell-derived SST annual amplitude again indicates reduced summer upwelling and an increased influence of westerly winds.

A similar pattern is observed in the trend of SST amplitudes over the MIS5/4 transition. Increasing sea-ice extent across the transition is accompanied by increasing annual SST amplitudes in the near-shore SST reconstructions at PP5-6. During levels LBSR (82 ± 4 ka) and ALBS (72 ± 3 ka) at PP5-6, annual SST amplitudes were lower than in the subsequent SADBS (71 ± 3 ka) and OBS1 (69 ± 3 ka) levels, suggesting a decrease in summer upwelling and an increased importance of westerly winds along the south coast, driven by expanded Antarctic sea-ice. However, the same pattern does not appear to hold in the MIS5 assemblages from KRM. While the two earliest assemblages (MSA I [115-120 ka] and MSA II lower [90 – 95 ka]) have equivalent annual SST amplitudes, the annual SST amplitude of MSA II upper (80 - 85 ka) is higher, suggesting a decrease in summer upwelling, yet sea-ice extent declines slightly across this period. However, the age ranges for the KRM deposits are not as well established as those of the other sites here – it is possible that ongoing dating studies at KRM will provide more precise and accurate age estimates for the deposits.

### 4.2 Near-shore SSTs and terrestrial precipitation trends

According to the Cohen and Tyson (1995) model, shifts in near-shore SST seasonality respond to seasonal, wind-driven upwelling (e.g. decreased seasonality as a result of decreased summer SSTs linked to wind-driven upwelling). The low annual SST amplitude during the mid-Holocene indicates that upwelling intensity was greatest during the mid-Holocene, which would correspond with increased summer rainfall. Environmental records from the summer rainfall region show that the mid-Holocene was indeed a time of generally moister conditions (Scott et al., 2012; Scott and Lee-Thorp, 2004). Warmer, moister conditions in the northern savanna region are reflected in the Makapansgat T7 speleothem between 6.4 – 5.1 ka (Holmgren et al., 2003; Lee-Thorp et al., 2001),

and high water levels are recorded in pans to the south, in the highveld grassland around Florisbad (Scott and Nyakale, 2002). Pollen records from the coastal Lake Eteza, at the eastern edge of the subcontinent, capture a moist episode between *c*. 7 – 4 ka, which Scott et al. (2012) hypothesise is linked to the warming of the Agulhas: instead, we suggest here that it reflects increased easterly winds that are also recorded in the seasonal SST record of upwelling.

In contrast, during the terminal Pleistocene Younger Dryas event from *c*. 13 – 11.5 ka, generally dry conditions prevailed across the southern African interior (Scott et al., 2012), and this is consistent with the SST record of increased seasonality which suggests a low frequency of summer upwelling and easterly component winds at this time. Similarly, Scott et al. (2012) note lower moisture levels recorded in pollen records from several sites in the SRZ during the late Holocene, *c*. 3.5 - 1.5 ka, which is also suggested by the rise in seasonality seen in the late Holocene shell SST record. The Holocene SST record thus aligns well with the expectations of the Cohen and Tyson (1995) model for the SRZ.

Detailed records of SRZ precipitation are scarce for earlier periods, but the similarity between the pattern of increasing SST amplitude recorded across the MIS5/4 transition with the mirrored trend for the terminal Pleistocene/Holocene, suggests a decrease in summer rainfall in the interior across the MIS5/4 transition. One of the few archives that spans this period, the Tswaing crater sedimentary record (Partridge et al., 1997) shows a decrease in summer rainfall between MIS5/4. An off-shore record of terrestrial run-off, situated off the east coast of South Africa, shows spikes in summer rainfall during late MIS5 (Ziegler et al., 2013). However, the nature of that record is such that it does not capture periods of increased aridity.

An indirect line of evidence for drying in the SRZ during MIS4 comes from off-shore records along the western coast that show increasing proportions of rainfall in the WRZ, particularly from *c*. 73 – 57 ka (Chase, 2010). An increase in winter rainfall would result if the westerly wind system was forced northwards, which is consistent with the increased seasonality seen in the shell SST record. A confounding factor for reconstructing precipitation from terrestrial archives is the effect of global temperature shifts on aridity across this time – although summer rainfall may have decreased during MIS4, the year-round rainfall region remained generally humid due to the cooler temperatures and larger amounts of winter rainfall (Chase, 2010; Chevalier and Chase, 2016).

## 5 Conclusions

Seasonal near-shore SSTs as reconstructed from serial $\delta^{18}O$ measurements of *Turbo sarmaticus* opercula collected from archaeological sites along the southernmost coast of South Africa correspond closely with global SST trends across MIS5, MIS4, the terminal Pleistocene and the Holocene. Largely stable SSTs across the interstadial periods of MIS5 are followed by sudden fluctuations in average SST across the MIS5/4 transition. From the terminal Pleistocene, average SSTs rise steadily through to the late Holocene, by a total of *c*. 4°C.

While seasonal insolation does not appear to correspond with the seasonality of near-shore SSTs, shifts in the annual SST amplitude may reflect wind-driven upwelling intensity, apparently in response to Antarctic sea-ice forcing of the westerly wind belt. Increased upwelling (as reflected in a low annual SST amplitude) during the mid-Holocene corresponds with increased precipitation in the summer rainfall region. Both increased upwelling intensity and summer precipitation amounts are predicted responses to an increased frequency of easterly component winds which bring moisture from the warm Agulhas and Indian Ocean. Conversely, reduced near-shore upwelling during the

terminal Pleistocene (as reflected in a high annual SST amplitude), when sea-ice was more extensive and the westerly wind systems were shifted equatorwards, corresponds with drier conditions over the summer rainfall zone. Similar, but mirrored, SST trends are observed across the MIS5/4 transition, in the PP5-6 assemblage. Increasing annual SST amplitude across the transition suggests a decrease in summer upwelling as sea-ice expanded around Antarctica. Such an expansion would force the westerly wind belt north, reducing the frequency of easterly component winds over the south coast and resulting in reductions in summer rainfall from MIS5 through to the start of MIS4.

This study augments the range of seasonal climate archives from a globally-important but poorly-understood system. More broadly, the approach taken here demonstrates the value of seasonally resolved near-shore SST records from archaeological marine molluscs for connecting marine and terrestrial climate systems. Oceanographic processes that primarily affect near-shore contexts should be distinguished from trends in the open ocean, as SST records from the two contexts are not equivalent. In this study, we link near-shore upwelling dynamics, as revealed in seasonal SST records, with regional precipitation trends, via latitudinal shifts in the rain-bearing wind systems (Cockcroft et al., 1987; Cohen and Tyson, 1995). Currently, the number of annual seasonal SST cycles represented in each depositional context is small for the purpose of defining average climate states, but given the large numbers of archaeological sites with well-preserved shell material along the South African coastline, the approach taken here offers good possibilities for developing detailed records of SST and precipitation shifts across the last glacial period for this region.

**Acknowledgments**

This work was supported by the South African Research Chairs Initiative of the Department of Science and Technology and the National Research Foundation of South Africa; Merton College, Oxford; a Quaternary Research Association New Research Worker's Award, the Palaeontological Scientific Trust and a NERC Isotopes Geosciences Facilities Steering Committee Award (grant number IP-1543-0515). Permissions for export and sampling were obtained from the curator of the archaeological collections at Iziko Museum, Heritage Western Cape (case number 14072110GT0730E) and the Eastern Cape Provincial Heritage Resources Agency (permit number 2/2/APM-PERMIT/14/09/003). Grateful acknowledgments to Curtis Marean and Sarah Wurz for help accessing the collections from PP5-6 and KRM. Thanks are also due to Gideon Henderson for access to sampling equipment in the Department of Earth Sciences, Oxford and especially to Chris Day, Peter Ditchfield, Hilary Sloane, Chris Richardson and Andy Gledhill for help with analyses.

589 **6 References**


590 Berger, A., Loutre, M.F., 1991. Insolation values for the climate of the last 10 million years. Quat. Sci.
591 Rev. 10, 297–317. doi:10.1016/0277-3791(91)90033-Q

592 Branch, G., Griffiths, C., Branch, M., Beckley, L., 2007. Two oceans: a guide to the marine life of
593 southern Africa, 2nd ed. Struik Publishers, Cape Town.

594 Bruton, J., Baird, D., Coetzee, P.S., 1991. Population structure and yield-per-recruit analysis of the
595 giant periwinkle Turbo sarmaticus in the Cape St Francis region, South Africa. South African J.
596 Mar. Sci. 11, 345–356. doi:10.2989/025776191784287754

597 Caley, T., Kim, J.-H., Malaizé, B., Giraudeau, J., Laepple, T., Caillon, N., Charlier, K., Rebaubier, H.,
598 Rossignol, L., Castañeda, I.S., Schouten, S., Sinninghe Damsté, J.S., 2011. High-latitude obliquity
599 as a dominant forcing in the Agulhas current system. Clim. Past 7, 1285–1296. doi:10.5194/cp-
600 7-1285-2011

601 Carré, M., Bentaleb, I., Fontugne, M., Lavallee, D., 2005. Strong El Nino events during the early
602 Holocene: stable isotope evidence from Peruvian sea shells. The Holocene 15, 42.
603 doi:10.1191/0959683605h1782rp

604 Chase, B.M., 2010. South African palaeoenvironments during marine oxygen isotope stage 4: a
605 context for the Howiesons Poort and Still Bay industries. J. Archaeol. Sci. 37, 1359–1366.
606 doi:10.1016/j.jas.2009.12.040

607 Chase, B.M., Lim, S., Chevalier, M., Boom, A., Carr, A.S., Meadows, M.E., Reimer, P.J., 2015. Influence
608 of tropical easterlies in southern Africa's winter rainfall zone during the Holocene. Quat. Sci.
609 Rev. 107, 138–148. doi:10.1016/j.quascirev.2014.10.011

610 Chevalier, M., Chase, B.M., 2016. Determining the drivers of long-term aridity variability: a southern
611 African case study. J. Quat. Sci. 31, 143–151. doi:10.1002/jqs.2850

612 Cockcroft, M.J., Wilkinson, M.J., Tyson, P.D., 1987. The application of a present-day climatic model to
613 the late Quaternary in southern Africa. Clim. Chang. 10, 161–181. doi:10.1007/BF00140253

614 Cohen, A., Tyson, P.D., 1995. Sea-surface temperature fluctuations during the Holocene off the
615 south coast of Africa: implications for terrestrial climate and rainfall. The Holocene 5, 304–312.
616 doi:10.1177/095968369500500305

617 Deacon, H.J., Geleijnse, V.B., 1988. The stratigraphy and sedimentology of the main site sequence,
618 Klasies River, South Africa. South African Archaeol. Bull. 43, 5–14. doi:10.2307/3887608

619 Deacon, J., 1986. The Later Stone Age of Southernmost Africa. University of Cape Town.

620 Ferguson, J.E., Henderson, G.M., Fa, D.A., Finlayson, J.C., Charnley, N.R., 2011. Increased seasonality
621 in the Western Mediterranean during the last glacial from limpet shell geochemistry. Earth
622 Planet. Sci. Lett. 308, 325–333. doi:10.1016/j.epsl.2011.05.054

623 Fischer, H., Fundel, F., Ruth, U., Twarloh, B., Wegner, A., Udisti, R., Becagli, S., Castellano, E.,
624 Morganti, A., Severi, M., Wolff, E., Littot, G., Röthlisberger, R., Mulvaney, R., Hutterli, M.A.,
625 Kaufmann, P., Federer, U., Lambert, F., Bigler, M., Hansson, M., Jonsell, U., Angelis, M. de,
626 Boutron, C., Siggaard-Andersen, M.-L., Steffensen, J.P., Barbante, C., Gaspari, V., 2007.
627 Reconstruction of millennial changes in dust emission, transport and regional sea ice coverage
628 using the deep EPICA ice cores from the Atlantic and Indian Ocean sector of Antarctica. Earth
629 Planet. Sci. Lett. 260, 340–354. doi:10.1016/j.epsl.2007.06.014

630 Fisher, E.C., Akkaynak, D., Harris, J., Herries, A.I.R., Jacobs, Z., Karkanas, P., Marean, C.W., McGrath,
631 J.R., 2015. Technical considerations and methodology for creating high-resolution, color-

632 corrected, and georectified photomosaics of stratigraphic sections at archaeological sites. J.
633 Archaeol. Sci. 57, 380–394. doi:10.1016/j.jas.2015.02.022

634 Foster, G., 1997. Growth, reproduction and feeding biology of Turbo sarmaticus (Mollusca:
635 Vetigastropoda) along the coast of the Eastern Cape Province of South Africa. Rhodes
636 University.

637 Foster, G., Hodgson, A., Balarin, M., 1999. Effect of diet on growth rate and reproductive fitness of
638 Turbo sarmaticus (Mollusca: Vetigastropoda: Turbinidae). Mar. Biol. 134, 307–315.
639 doi:10.1007/s002270050548

640 Füllenbach, C.S., Schöne, B.R., Mertz-Kraus, R., 2015. Strontium/lithium ratio in aragonitic shells of
641 Cerastoderma edule (Bivalvia)—A new potential temperature proxy for brackish environments.
642 Chem. Geol. 417, 341–355.

643 Galimberti, M., 2010. Investigating the use of oxygen and carbon isotopes and sclerochronology on
644 Turbo sarmaticus and Donax serra for palaeoenvironment reconstruction at Pinnacle Point,
645 South Africa. University of Cape Town.

646 Galimberti, M., Loftus, E., Sealy, J.C., 2016. Investigating δ18O of Turbo sarmaticus (L. 1758) as an
647 indicator of sea surface temperatures. Palaeogeogr. Palaeoclimatol. Palaeoecol. in press.

648 Grossman, E., Ku, T., 1986. Oxygen and carbon isotope fractionation in biogenic aragonite:
649 temperature effects. Chem. Geol. Isot. Geosci. Sect. 59, 59–74. doi:10.1016/0168-
650 9622(86)90057-6

651 Henshilwood, C.S., 2008. Holocene prehistory of the southern Cape. Excavations at Blombos Cave
652 and Blombosfontein Nature Reserve. BAR International Series 1860. Cambridge Monographs in
653 African Archaeology, 75, Cambridge.

654 Holmgren, K., Lee-Thorp, J.A., Cooper, G.R.J., Lundblad, K., Partridge, T.C., Scott, L., Sithaldeen, R.,
655 Talma, S.A., Tyson, P.D., 2003. Persistent millennial-scale climatic variability over the past
656 25,000 years in Southern Africa. Quat. Sci. Rev. 22, 2311–2326. doi:10.1016/S0277-
657 3791(03)00204-X

658 Hudson, J.D., Anderson, T.F., 1989. Ocean temperatures and isotopic compositions through time.
659 Trans. R. Soc. Edinb. Earth Sci. 80, 183–192. doi:10.1017/S0263593300028625

660 Karkanas, P., Brown, K.S., Fisher, E.C., Jacobs, Z., Marean, C.W., 2015. Interpreting human behavior
661 from depositional rates and combustion features through the study of sedimentary microfacies
662 at site Pinnacle Point 5-6, South Africa. J. Hum. Evol. 85, 1–21.
663 doi:10.1016/j.jhevol.2015.04.006

664 Kim, S.-T., Mucci, A., Taylor, B., 2007. Phosphoric acid fractionation factors for calcite and aragonite
665 between 25 and 75 °C: Revisited. Chem. Geol. Isot. Geosci. 246, 135–146.

666 Kyriacou, K., 2009. The reinvestigation of Hoffman's/Robberg Cave - the artefactual and shellfish
667 assemblages. University of Cape Town.

668 Langejans, G.H.J., Niekerk, K. van, Dusseldorp, G.L., Thackeray, J.F., 2012. Middle Stone Age shellfish
669 exploitation: Potential indications for mass collecting and resource intensification at Blombos
670 Cave and Klasies River, South Africa. Quat. Int. 270, 80–94. doi:10.1016/0168-9622(86)90057-6

671 Lee-Thorp, J.A., Holmgren, K., Lauritzen, S.E., Linge, H., Moberg, A., Partridge, T.C., Stevenson, C.,
672 Tyson, P.D., 2001. Rapid climate shifts in the southern African interior throughout the mid to
673 late Holocene. Geophys. Res. Lett. 28, 4507–4510. doi:10.1029/2000GL012728

674 Loftus, E., Rogers, K., Lee-Thorp, J.A., 2015. A simple method to establish calcite:aragonite ratios in

675 archaeological mollusc shells. J. Quat. Sci. 30, 731–735. doi:10.1002/jqs.2819

676 Loftus, E., Sealy, J.C., Lee-Thorp, J.A., 2016. New Radiocarbon Dates and Bayesian Models for Nelson
677 Bay Cave and Byneskranskop 1: Implications for the South African Later Stone Age Sequence.
678 Radiocarbon 58, 365–381. doi:10.1017/RDC.2016.12

679 Partridge, T.C., Demenocal, P.B., Lorentz, S.A., Paiker, M., Vogel, J.C., 1997. Orbital forcing of climate
680 over South Africa: a 200.000-year rainfall record from the Pretoria Saltpan. Quat. Sci. Rev. 16,
681 1125–1133.

682 Schumann, E., 1999. Wind-driven mixed layer and coastal upwelling processes off the south coast of
683 South Africa. J. Mar. Res. 57, 671–691. doi:10.1357/002224099321549639

684 Schumann, E., Cohen, A., Jury, M.R., 1995. Coastal sea surface temperature variability along the
685 south coast of South Africa and the relationship to regional and global climate. J. Mar. Res. 53,
686 231–248. doi:10.1357/0022240953213205

687 Schweitzer, F.R., Wilson, M., 1982. Byneskranskop 1: A Late Quaternary living site in the southern
688 Cape Province. Ann. South African Museum 88, 1–102.

689 Scott, L., Lee-Thorp, J.A., 2004. Holocene climatic trends and rhythms in Southern Africa, in:
690 Battarbee, R.W., Gasse, F., Stickley, C.E. (Eds.), Past Climate Variability through Europe and
691 Africa. Springer Netherlands, Amsterdam, pp. 69–91.

692 Scott, L., Neumann, F.H., Brook, G.A., Bousman, C.B., Norström, E., Metwally, A.A., 2012. Terrestrial
693 fossil-pollen evidence of climate change during the last 26 thousand years in Southern Africa.
694 Quat. Sci. Rev. 32, 100–118. doi:10.1016/j.quascirev.2011.11.010

695 Scott, L., Nyakale, M., 2002. Pollen indications of Holocene palaeoenvironments at Florisbad in the
696 Central Free State, South Africa. The Holocene 14, 497–503. doi:10.1191/0959683602hl563rr

697 Shackleton, N., 1982. Stratigraphy and chronology of the KRM deposits: oxygen isotope evidence.,
698 in: Singer, R., Wymer, J.J. (Eds.), The Middle Stone Age at Klasies River Mouth in South Africa.
699 University of Chicago, Chicago, pp. 192–199.

700 Simon, M.H., Arthur, K.L., Hall, I.R., Peeters, F.J.C., Loveday, B.R., Barker, S., Ziegler, M., Zahn, R.,
701 2013. Millennial-scale Agulhas Current variability and its implications for salt-leakage through
702 the Indian-Atlantic Ocean Gateway. Earth Planet. Sci. Lett. 383, 101–112.
703 doi:10.1016/j.epsl.2013.09.035

704 Tyson, P.D., Preston-Whyte, R., 2000. The weather and climate of southern Africa. Oxford University
705 Press, Cape Town.

706 Urey, H., Lowenstam, H.A., Epstein, S., McKinney, C.R., 1951. Measurement of paleotemperatures
707 and temperatures of the Upper Cretaceous of England, Denmark, and the southeastern United
708 States. Geol. Soc. Am. Bull. 62, 399. doi:10.1130/0016-7606(1951)62[399:MOPATO]2.0.CO;2

709 van Andel, T.H., 1989. Late Pleistocene Sea Levels and the Human Exploitation of the Shore and Shelf
710 of Southern South Africa. J. F. Archaeol. 16, 133–155. doi:10.1179/jfa.1989.16.2.133

711 Waelbroeck, C., Labeyrie, L., Michel, E., Duplessy, J.C., McManus, J.F., Lambeck, K., Balbon, E.,
712 Labracherie, M., 2002. Sea-level and deep water temperature changes derived from benthic
713 foraminifera isotopic records. Quat. Sci. Rev. 21, 295–305. doi:10.1016/S0277-3791(01)00101-9

714 Wurz, S., 2002. Variability in the middle stone age lithic sequence, 115,000-60,000 years ago at
715 Klasies river, South Africa. J. Archaeol. Sci. 29, 1001–1015. doi:10.1006/jasc.2001.0799

716 Ziegler, M., Simon, M., Hall, I., Barker, S., Stringer, C.B., Zahn, R., 2013. Development of Middle Stone

717 Age innovation linked to rapid climate change. Nat. Commun. 4, 1905.
718 doi:10.1038/ncomms2897

719

## 7 Supplementary figures

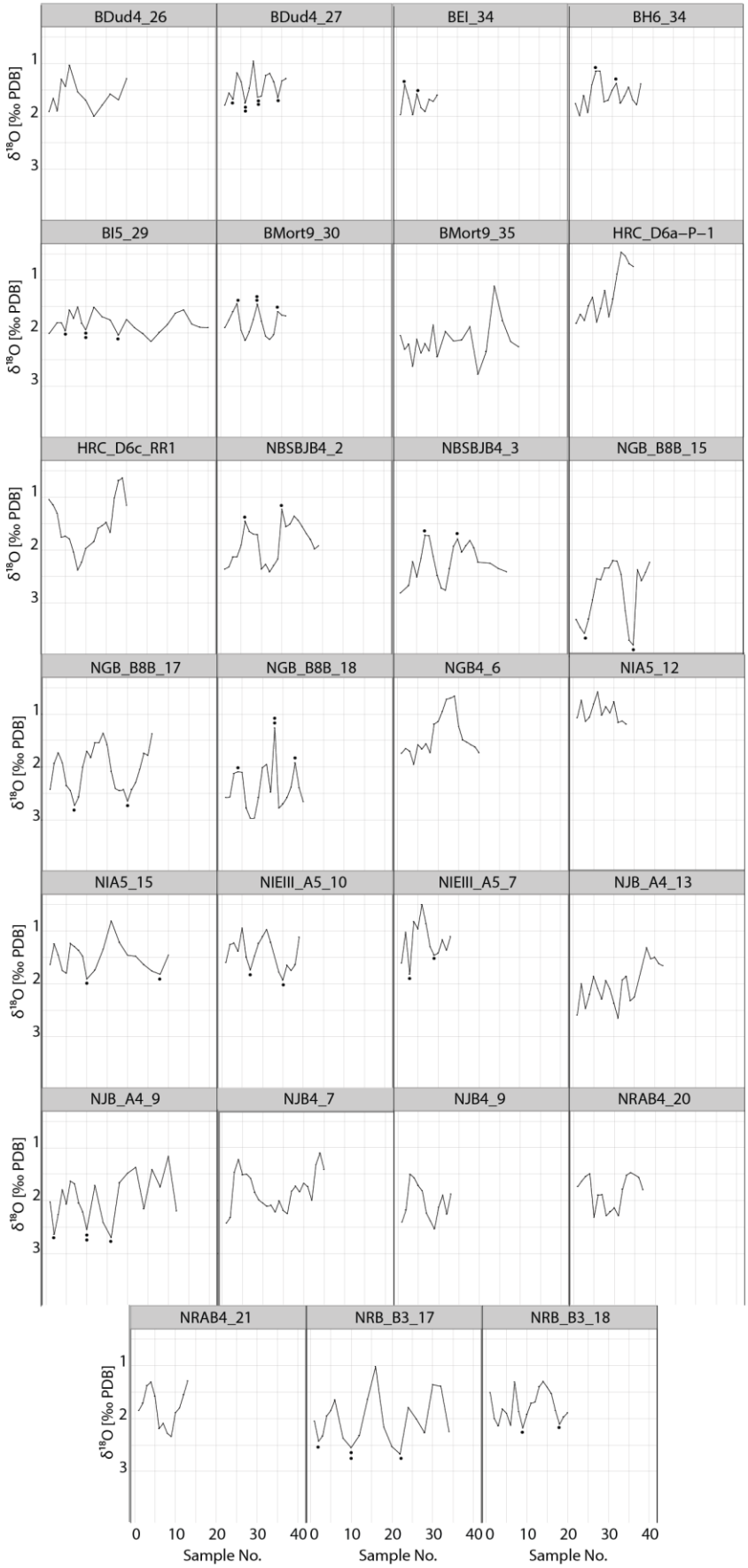


**SM Figure 1** Serial $\delta^{18}O$ sequences from twenty-seven Holocene and Pleistocene aged *Turbo sarmaticus* opercula (see Table 1 for context).

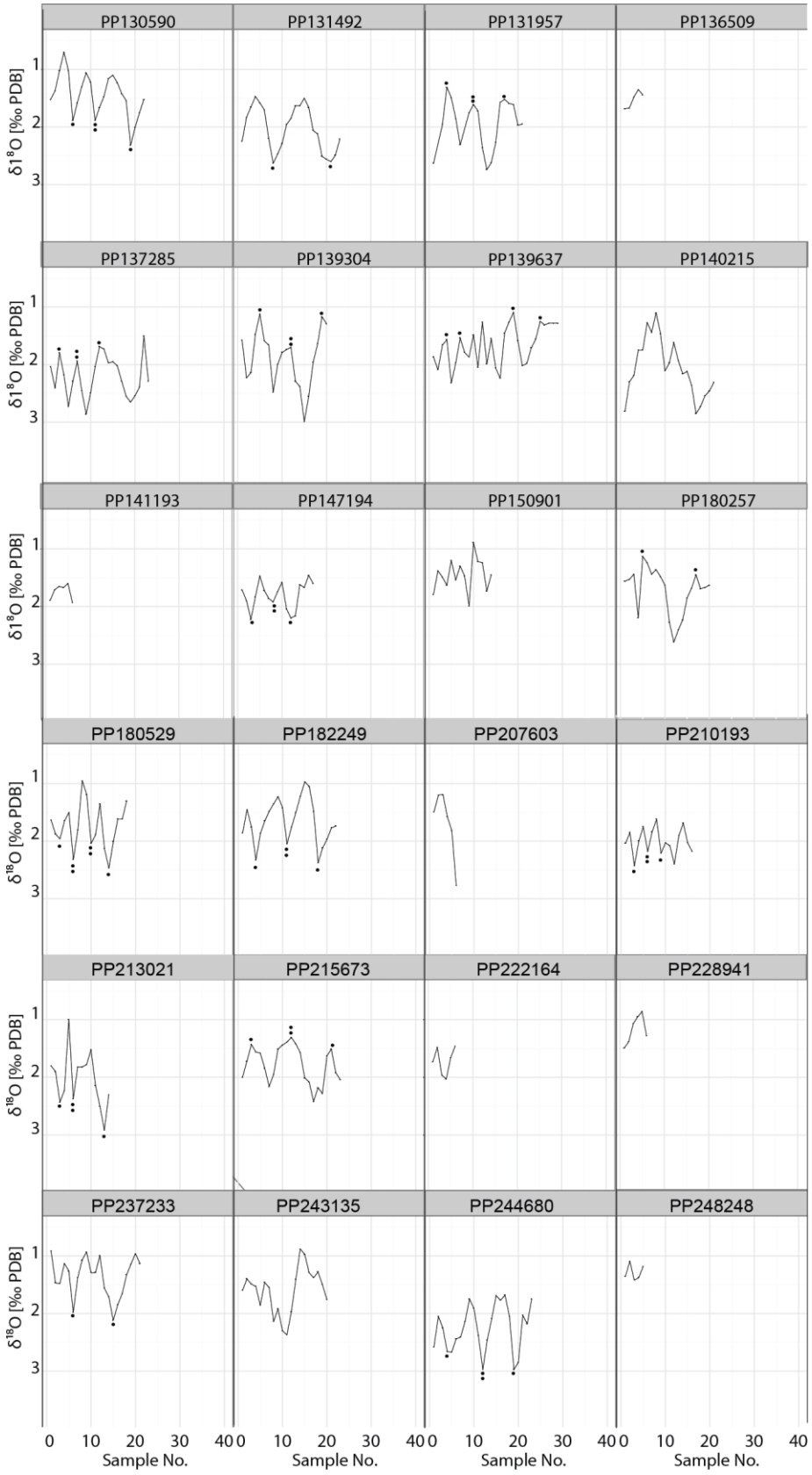


724

725 **SM Figure 2** Serial $\delta^{18}O$ sequences from twenty-four *Turbo sarmaticus* opercula from Pinnacle Point
726 5-6 (see Table 1 for context of each shell).

727

728

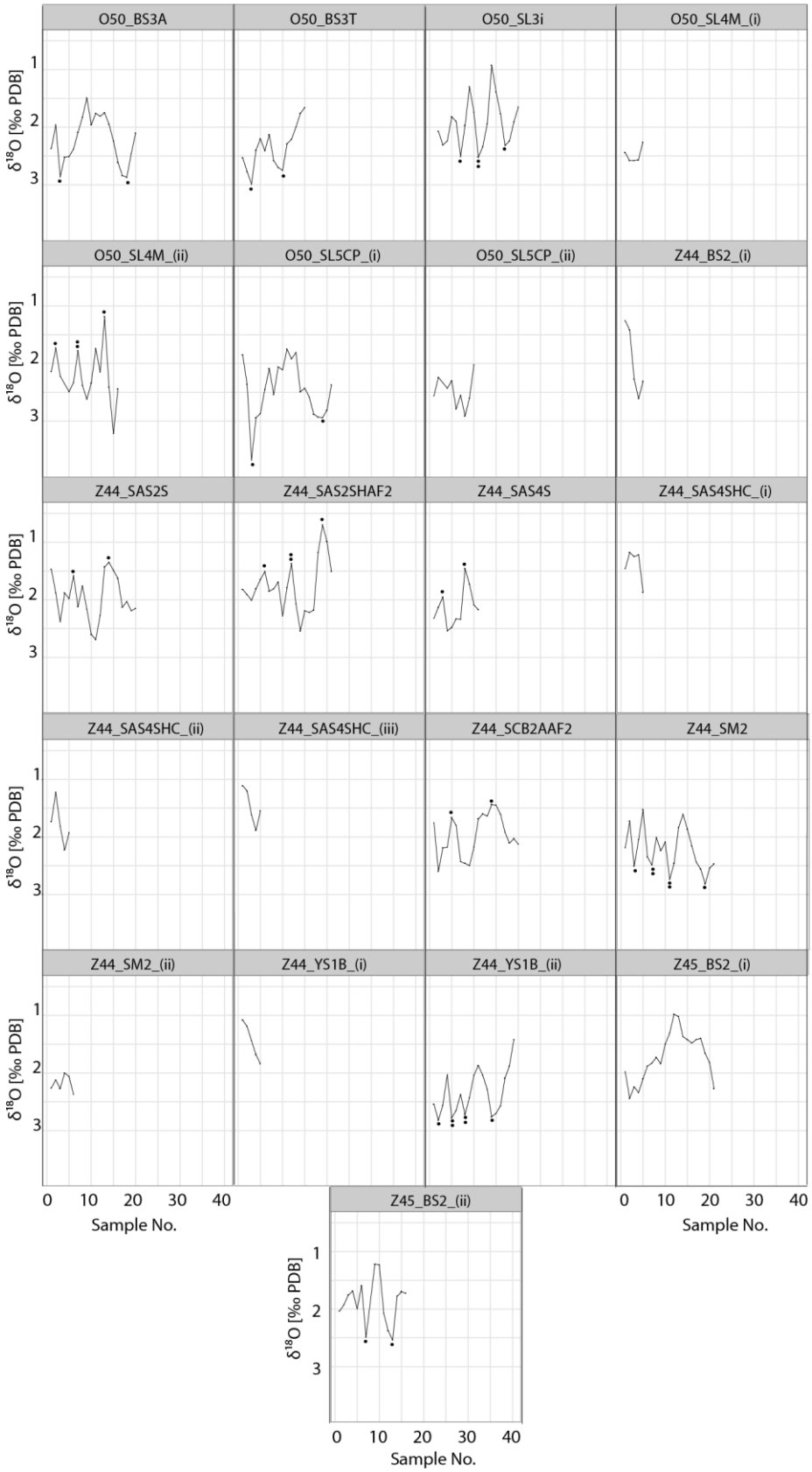


729

730 **SM Figure 3** Serial $\delta^{18}O$ sequences from twenty-one *Turbo sarmaticus* opercula from Klasies River
731 main site (see Table 1 for context of each shell).